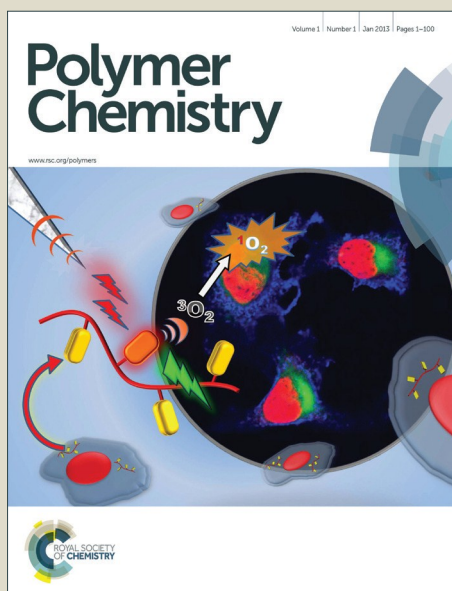


Polymer Chemistry

Accepted Manuscript



This is an *Accepted Manuscript*, which has been through the Royal Society of Chemistry peer review process and has been accepted for publication.

Accepted Manuscripts are published online shortly after acceptance, before technical editing, formatting and proof reading. Using this free service, authors can make their results available to the community, in citable form, before we publish the edited article. We will replace this *Accepted Manuscript* with the edited and formatted *Advance Article* as soon as it is available.

You can find more information about *Accepted Manuscripts* in the [Information for Authors](#).

Please note that technical editing may introduce minor changes to the text and/or graphics, which may alter content. The journal's standard [Terms & Conditions](#) and the [Ethical guidelines](#) still apply. In no event shall the Royal Society of Chemistry be held responsible for any errors or omissions in this *Accepted Manuscript* or any consequences arising from the use of any information it contains.

ARTICLE

High performance quinacridone-based polymers in film transistors and photovoltaics: effect of vinylene linkage on crystallinity and morphology

Cite this: DOI: 10.1039/x0xx00000x

Hui Li,^{a,b} Xuedong Wang,^{a,b} Fangbin Liu,^{a,b} and Hongbing Fu^{*a,c}Received 00th January 2012,
Accepted 00th January 2012

DOI: 10.1039/x0xx00000x

www.rsc.org/

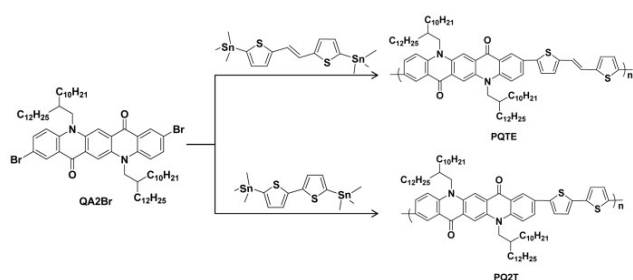
A novel quinacridone-based polymer containing vinylene linkage, **PQTE**, was synthesized and exhibited higher performance both in organic thin-film transistor and solar cell than that of the reference polymer **PQ2T**. Introducing the vinylene linkage, strong interchain interaction is obtained with short π - π stacking distance of 3.49 Å in polymer **PQTE**, which is responsible for the highest mobility of 0.67 cm² V⁻¹ s⁻¹ reported to date for quinacridone-based semiconductors. More significantly, the incorporation of thienylene-vinylene-thienylene unit contributes to good miscibility between **PQTE** and PC₇₁BM. Because of the effective intercalation of PC₇₁BM in the **PQTE** lamellar structure, high power conversion efficiency of 3.9% was achieved without any additives or post-treatments. Our rational molecular design qualifies quinacridone as a promising building block simultaneously in high performance polymer thin-film transistor and solar cell.

Introduction

Recent interests in polymer semiconductors are motivated by their potential application in large-area and roll-to-roll organic electronics like organic thin-film transistors (OTFT) and organic photovoltaics (OPV).^{1,2} Molecular engineering of polymers allows for the adjustment of photo/electrochemical properties, solubility, packing, morphology of thin film and thus achievement of high performance.^{3,4} The common structural feature of these polymer semiconductors is alternating electron-rich (donor) and electron-deficient (acceptor) units linked along polymer chains.^{5,6} Over the years, great efforts have been given to the search of efficient donor or acceptor units and the combination between these units. Impressive power conversion efficiency (PCE) of >8% in OPV⁷⁻⁹ and remarkable mobility of >10 cm² V⁻¹ s⁻¹ in OTFT¹⁰⁻¹² have been achieved by incorporating attractive units, such as benzodithiophene, diketopyrrolopyrrole, benzothiadiazole, isoindigo and arylene diimides, etc. Among these remarkable works on OPV devices, cosolvents, small-molecule additives, and post-treatments, such as thermal annealing and solvent-vapour annealing, have been proved useful strategies to improve microstructure of blend films. Unfavourably, these additional processes increase fabrication cost and are unable to fulfill commercial requirements. Therefore, the development of new building blocks with excellent properties both in photonics and electronics, as well as a simple fabrication process, is still a major challenge for material chemists.¹³

Recently, we have paid much attention to the quinacridone (QA) units. It is a five-ring planar structure and widely used as the magenta toner with excellent stability.¹⁴⁻¹⁷ That the nitrogen atoms can be functionalized with alkyl groups make it possible using in photoelectrical devices via solution processibility. However, to the best of our knowledge, only numerable works are reported in the field of OTFT^{18,19} and OPVs^{15, 20-24} based on this unit. In our group, we have reported polymer PQBOC8 containing QA and benzothiadiazole,²⁵ although the effective conjugation is limited along polymer backbone, this polymer still exhibited reasonable hole mobility in OFET and high PCE in OPV, simultaneously.²³ Moreover, the crystalline ultra-thin film of this polymer showed high photoresponsivity.²⁶ These encouraging results indicate that QA would be a promising building block for semiconducting polymers. Nevertheless, the mobilities of all these reported QA-based polymers are relative low because of large π - π stacking distance (~ 4 Å).²⁷ On the other hand, despite using additives or post-treatment methods, the PCE of QA-based polymers is still limited to 2-3%.^{24,27} Therefore, rational design of polymer backbone for QA-based polymers is urgently needed for further advancement in optoelectronic performance.

On the basis of above consideration, we firstly introduce vinylene linkage into QA-containing polymer, namely **PQTE**. In view of its rigid and transconfiguration, thienylene-vinylene-thienylene in polymer **PQTE** is expected to result in much planar configuration and strong interchain interaction.^{28,29} For



Scheme 1 Chemical structures and synthetic routes of quinacridone-based copolymers

comparison, polymer **PQ2T** containing QA and bithiophene was also synthesized. As a result, the introduction of vinylene linkage improves not only the crystallinity of thin films but also the miscibility with PC₇₁BM. In OTFTs, **PQTE** film exhibited a short π - π stacking distance of 3.49 Å and high mobility up to 0.67 cm² V⁻¹ s⁻¹. In solar cell, as donor material, **PQTE** exhibited PCE up to 3.9% because of the better miscibility with PC₇₁BM than that of **PQ2T** though **PQTE** showed stronger intermolecular interaction. It is noteworthy that the PCE of **PQTE** is among the highest performance for QA-based polymers even though these devices were fabricated without any additives or post-treatments.

Results and discussion

Synthesis and characterization

The synthetic routes of two polymers are shown in Scheme 1. Monomer QA2Br was synthesized according to our previous work.²⁵ The Stille-coupling reaction between monomer QA2Br and (*E*)-1,2-bis(5-(trimethylstannyl)thiophene-2-yl)ethene afforded polymer **PQTE**, while monomer QA2Br reacted with 5,5'-bis(trimethylstannyl)-2,2'-bithiophene via same reaction conditions obtained polymer **PQ2T** for comparison. Both of polymers are purified by successive Soxhlet extractions. More detailed descriptions of the synthesis are available in the experimental section. Two polymers have almost identical number-average molecular weight ($M_n = 20.60$ kDa for **PQTE** and $M_n = 20.11$ kDa for **PQ2T**) with very low polydispersity indexes (PDI) close to 1, as shown in Table 1, Fig. S1† and Fig. S2†. Two polymers showed very good thermal stability which were determined by thermogravimetric analysis (TGA). **PQTE** showed little lower decomposition temperature T_d of 405.3 °C while **PQ2T** exhibited a higher T_d up to 436.3 °C (Fig. S3†). Differential scanning calorimetry (DSC) was employed to investigate the thermal transition of polymers. No obvious thermal transition peak was observed in the range of 25-300 °C for two polymers before decomposition, which is probably attributed to the rigid backbone limiting the chain motion.³⁰

Optical and electronic properties

The absorption spectra of two polymers both in dilute chloroform solution and in solid state are shown in Fig. 1 and relevant data are summarized in Table 1. Compared with **PQ2T**,

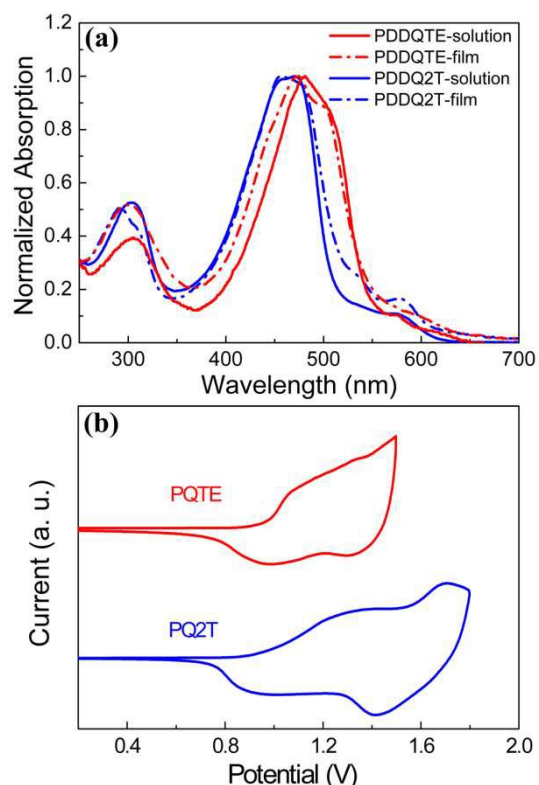


Fig. 1 (a) Normalized absorption of two polymers in dilute CHCl₃ solution (solid line) and in film (dash-dot line). (b) Cyclic voltammograms of **PQTE** and **PQ2T** films in 0.1 M [tBu₄N]⁺[PF₆]⁻ acetonitrile solution at a scan rate of 50 mV s⁻¹.

PQTE showed red-shift absorption both in solution and thin film owing to extended π -conjugation induced by integration of vinylene linkage. For **PQ2T**, the maximum absorption peak was featureless and no obvious spectral shift was observed in solid state compared with that in dilute solution, indicating the polymer might form pre-aggregates in solution.³¹ In the case of polymer **PQTE**, the maximum absorption profile was significantly sharper and there was a prominent shoulder peak at longer wavelength (~499 nm). Moreover, the shoulder peak became much finer and stronger in thin film, which demonstrates that vinylene linkage in **PQTE** lead to much strongly aggregate in solid state. However, a slightly bathochromic shift (~10 nm) was observed going from solution to thin film for **PQTE** which was also observed in other polymers.³² Density-functional theory (DFT, B3LYP/6-31G) was performed to model the electron density distributions of two trimers, as shown in Fig. S4. From their highest occupied molecular orbital (HOMO) and lowest unoccupied molecular orbital (LUMO), we can observe that QA unit exhibited weak electro-deficient character and HOMO is not delocalized over the whole backbone.¹⁹ This is consistent with the fact that the weak shoulder peaks at around 550–630 nm can be attributed to intramolecular charge transfer (ICT). Because of weak electro-deficient character of quinacridone unit, the reduction curves cannot be determined, only oxidation curve are provided in Fig. 1b. The HOMO levels of **PQTE** and **PQ2T** calculated from the

Table 1 Molecular weights, optical properties, and energy levels of **PQTE** and **PQ2T**

polymer	M_n (kDa)	PDI	T_d (°C)	λ_{max} (nm)		HOMO ^a (eV)	LUMO ^b (eV)	$E_g^{opt,c}$ (eV)
				solution	film			
PQTE	20.60	1.15	405.3	481, 499, 576	471, 497, 574	-5.26	-3.38	1.88
PQ2T	20.11	1.13	436.3	471, 574	473, 578	-5.25	-3.28	1.97

^a Calculated from cyclic voltammetry curves. ^b Determined by LUMO = HOMO + E_g^{opt} . ^c Determined from the onset of the thin-film absorption.

onset oxidation potential³³ are almost identical (-5.3 eV) and approximated work function of gold. This indicates that hole injection will be easy from the gold electrode to polymers. Using their optical band gaps, the LUMO levels are calculated to be -3.38 eV and -3.28 eV for **PQTE** and **PQ2T**, respectively. Similar HOMO and LUMO energy levels indicate the incorporation of vinylene linkage cannot significantly influence the electrochemical properties of polymers.

OFET properties

To probe how the incorporation of vinylene linkage affects the charge transport of **PQTE**, bottom-gate/top-contact transistors were fabricated with channel length of 30 μm and channel width of 500 μm . The insulator was 300 nm SiO_2 layer passivated with octyltrichlorosilane (OTS). Polymer solution was heated and stirred at 80 °C for 5 hours before spin-coated on the substrate. The film thickness was about 35-40 nm. All films were annealed at 150 °C for 30 min. Au was used as source and drain electrodes by vacuum deposition. Fig. 2 shows the typical output and transfer curves of FETs based on two polymers. Carrier transport performances are summarized in Table 2. **PQTE** based FETs exhibit a maximum hole mobility as high as 0.67 $\text{cm}^2 \text{V}^{-1} \text{s}^{-1}$ with the average value of 0.54 $\text{cm}^2 \text{V}^{-1} \text{s}^{-1}$ and high on/off ratio (I_{on}/I_{off}) of 10^6 - 10^7 . This value is the highest mobility reported so far for quinaclidone-based

Table 2 Charge transport properties of **PQTE** and **PQ2T**

polymer	μ_{th} ($\text{cm}^2 \text{V}^{-1} \text{s}^{-1}$)		I_{on}/I_{off}	V_T (V)
	max	ave		
PQTE	0.67	0.54±0.09	10^6 - 10^7	-9.8
PQ2T	0.30	0.28±0.02	10^6 - 10^7	-12.0

Maximum and average mobilities are collected from more than 10 devices.

polymers. For **PQ2T**-based FETs, the highest mobility is calculated to be 0.30 $\text{cm}^2 \text{V}^{-1} \text{s}^{-1}$ with the average value of 0.28 $\text{cm}^2 \text{V}^{-1} \text{s}^{-1}$ and I_{on}/I_{off} of 10^6 - 10^7 , which is slightly higher than reported value by Kazuo Takimiya group. We attribute this enhancement to the lower PDI of **PQ2T** in our work. Smaller threshold voltages (V_T) are also observed for **PQTE** devices (-9.8 V) than those of **PQ2T** devices (-12.0 V). The high mobility and low V_T of TFTs based on **PQTE** are perhaps due to the preferable orientation of **PQTE** film.

Ordering structure of OFET film

To shed light on the structural effect by introduction of vinylene linkage into **PQTE**, geometry optimization and molecular ordering were determined by DFT and two-dimensional grazing incidence X-ray diffraction (2D-GIXRD), respectively. The dihedral angle in **PQTE** trimers is slightly smaller than that of **PQ2T** trimers suggesting better coplanar structure in **PQTE** (Fig. S4). Comparing the XRD pattern of two polymer films, as shown in Fig. 3, both polymer **PQTE** and **PQ2T** show ($h00$) diffractions up to the fourth order indicating these polymers are long-range-ordered. However, large arcing diffraction of **PQ2T** suggested that there is no preferential orientation in the film which is consistent with the reference 19. In contrast, the film of **PQTE** shows much centralized points along q_z axis and distinctly observable (010) diffraction along q_{xy} axis. The results indicate that the film of **PQTE** formed preferentially ordered edge-on orientation on the substrate.³⁴ The lamellar distances calculated from the out of plane pattern (Fig. 3c and Table S1) are 21.6 Å and 22.7 Å for **PQTE** and **PQ2T**, respectively. Shorter lamellar distance of **PQTE** means that alkyl chains are packed more intensely between adjacent polymer chains than those of **PQ2T**. From in plane pattern, **PQTE** shows strong (010) reflection peak corresponding to π - π stacking distance of 3.49 Å which is one of the shortest distances for polymers containing QA unit. For

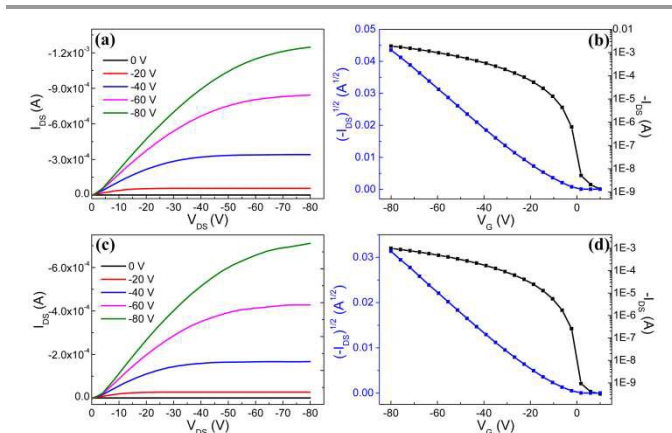


Fig. 2 Output (a, c) curves of **PQTE** and **PQ2T**, respectively. Transfer (b, d) curves of **PQTE** and **PQ2T** at $V_{ds} = -80$ V, respectively.

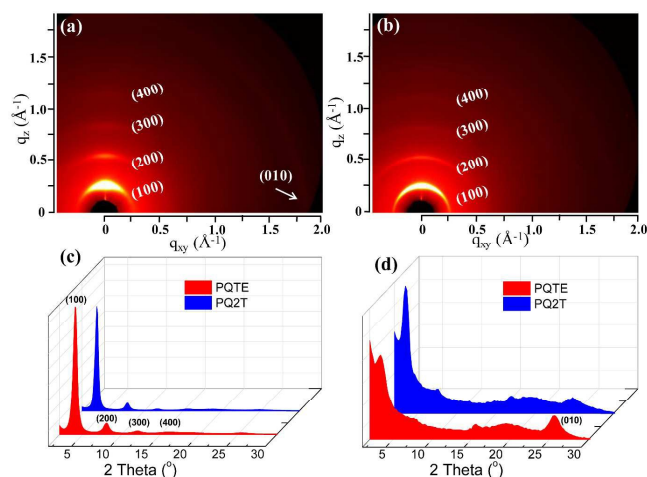


Fig. 3 2D-GIXRD patterns of the annealed **PQTE** film (a) and **PQ2T** film (b), respectively. Out of plane (c) and in plane GIXRD patterns of two polymers.

PQ2T film, weak (010) reflection peak could be observed in the out of plane with the corresponding π - π stacking distance of 3.59 Å. Moreover, the presence of (h00) peaks corresponding to lamellar structure further confirms that both face-on and edge-on orientations exist in this polymer film. Tapping-mode atomic force microscopy (AFM) further demonstrated the difference of morphology between two polymers (Fig. S5). **PQTE** film exhibit uniform intertwined fibre structures with obviously crystalline zones, which is the result of strong intermolecular interaction. In contrast, **PQ2T** film shows nodule-like morphology with relatively loose packed grains. According to the result mentioned above, it is confirmed that the insert of vinylene linkage shortens the π - π stacking distance of adjacent polymer chains because of good planarity and extended π -conjugation of vinylene linkage. Strong interchain interaction improves the crystallinity of **PQTE** film. These observations are in good agreement with the mobility analysis.

Solar cell properties

Bulk heterojunction solar cells were fabricated by employing **PQTE** or **PQ2T** as an electron donor and PC₇₁BM as an electron acceptor. The typical device configuration is ITO/PEDOT:PSS/polymer:PC₇₁BM/Ca/Al. J - V curves of the optimized photovoltaic devices are shown in Fig. 4a and the external quantum efficiency (EQE) spectra are displayed in Fig. 4b. The solar cell parameters are collected in Table 3 and Table S2. The optimum polymer:PC₇₁BM ratio was found to be 1:2. The blend solution was spin coated in chlorobenzene at 1000 rpm for 30 s. The thickness of active layer is about 100-115 nm. Note that no processing additives were used at the time of spin coating. Even without any post-treatment, the highest PCE for **PQTE** was 3.90% with a J_{sc} of 9.74 mA cm⁻², a V_{oc} of 0.73 V and a modest FF of 55%. For **PQ2T**, the devices exhibited a moderate PCE of 2.71% with a slightly increase in V_{oc} (0.74 V) and FF (56%) but lower J_{sc} of 6.95 mA cm⁻² compared with **PQTE**-based devices. It is noteworthy that PCE of 3.90% is among the highest efficiency reported for quinacridone-based

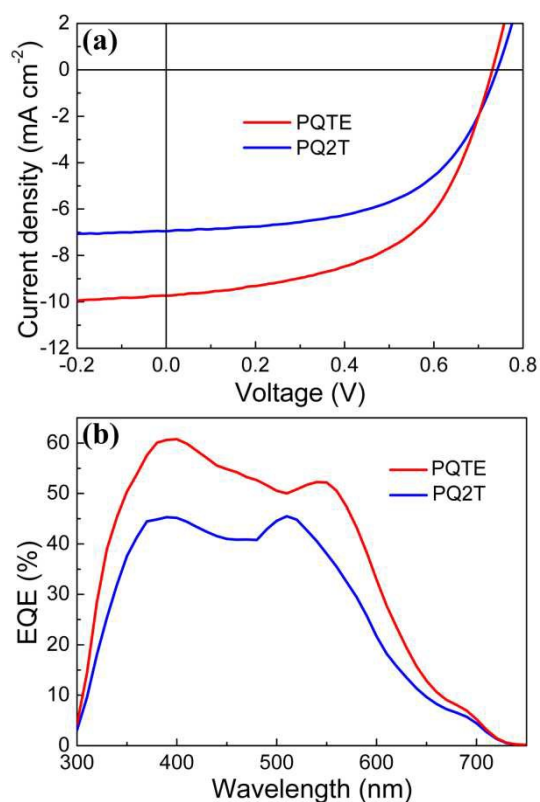


Fig. 4 J - V characteristics (a) and external quantum efficiency (EQE) spectra (b) of optimal solar cells from blend films of **PQTE**/PC₇₁BM and **PQ2T**/PC₇₁BM.

Table 3 Photovoltaic properties of solar cells based on polymer/PC₇₁BM

polymer ^a	V_{oc} (V)	J_{sc} (mA cm ⁻²)	FF (%)	PCE ^b (%)
PQTE	0.73	9.74	55	3.90 (3.79±0.09)
PQ2T	0.74	6.95	56	2.71 (2.62±0.12)

^a The weight ratio of polymer to PC₇₁BM is 1:2. ^b The value out of brackets represents maximum PCE; The value in brackets represents average values of PCE collected more than 10 devices.

polymers via simple device architecture without any additives or post-treatments, which are unique properties of **PQTE**. In Fig. 4b, high photo-to-current responses were obtained in the range from 350 to 600 nm for two polymer/PC₇₁BM blend films. For **PQTE**-based devices, the higher response verified higher J_{sc} value which supports the results from J - V characteristics.

Film morphology and microstructure in solar cell

The morphology of active layers was examined by bright field transmission electron microscopy (TEM) and AFM, respectively. In Fig. 5a, well distributed nano-fibrillar structures are observed in **PQTE**/PC₇₁BM blend film. This interpenetrating network is beneficial for charge dissociation.³⁵ For **PQ2T**-based device, macrophase separation limits the probability of exciton dissociation leading to poor J_{sc} (Fig. 5b). Additively, the results of AFM images (Fig. S6) reveal that the grains in **PQTE**/PC₇₁BM blend film are fairly homogeneous in

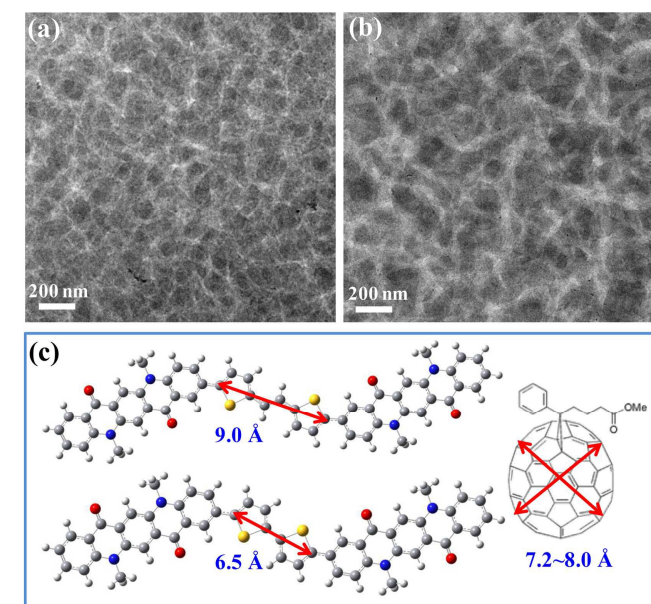


Fig. 5 Bright field TEM images of the optimized **PQTE/PC₇₁BM** blend film (a) and **PQ2T/PC₇₁BM** blend film (b). Calculated molecular configuration and sizes by DFT method (c). The alkyl substituents are replaced with the methyl group to simplify the calculation.

size and shape. However, the **PQ2T/PC₇₁BM** blend film shows large aggregates and the size is about 200-300 nm, indicating the poor dispersion of **PC₇₁BM** in the polymer matrix. We note that pure film of **PQTE** shows a higher degree of crystallinity and order than film of **PQ2T**. What's more, the polymer chains are closer than those of **PQ2T**. However, **PQTE** unexpectedly exhibits better miscibility with **PC₇₁BM** while **PQ2T/PC₇₁BM** blend film is apt to aggregate into large domains. This result could be explained by using DFT calculation and the experimental data collected from 2D-GIXRD of blend films. In blend films, thiophene-vinylene-thiophene (TVT) or bithiophene (BT) as donor unit in polymers backbone would interact with electro-deficient **PC₇₁BM** via electrostatic interaction. In consideration of the length of donor units (Fig. 5c), TVT unit with a length of 9.0 Å is larger than the size of **PC₇₁BM** (7.2~8.0 Å),³⁶ which provides enough volume to accommodate the fullerene molecules. In contrast, short BT unit (6.5 Å) would expel the fullerene resulting in self-aggregation of polymer chains and large domains of **PC₇₁BM**.³⁷ This is further confirmed by the results of 2D-GIXRD. As shown in Fig. S7 and Table S3, in **PQTE/PC₇₁BM** blend film, the lamellar distance shows 2.5 Å larger than that of in the polymer-only film. The significant increase indicates that **PC₇₁BM** molecules probably intercalate on the crystal lattice of **PQTE** because of sufficient volume.³⁸ In contrast, the lamellar distance of **PQ2T/PC₇₁BM** blend film exhibits negligible increases of 0.2 Å compared with the polymer-only film suggesting that **PC₇₁BM** molecules cannot intercalate well on **PQ2T**. As a result, good intercalation of **PC₇₁BM** into the lamellar structure of **PQTE** is responsible for this high PCE.

Conclusions

We synthesized a novel quinacridone-based polymer, **PQTE**, containing thiophene-vinylene-thiophene unit. **PQ2T** without vinylene linkage was also synthesized for comparison. As a result, the incorporation of vinylene linkage can efficiently shorten π - π stacking distance and improve the crystallinity of thin film. In TFTs, strong intermolecular interaction of **PQTE** enhances the charge carrier mobility up to $0.67 \text{ cm}^2 \text{ V}^{-1} \text{ s}^{-1}$. In solar cell, high PCE of 3.9% was obtained by using **PQTE** as donor and **PC₇₁BM** as acceptor while **PQ2T**-based devices showed moderate PCE of 2.70%. It is noteworthy that high PCE were obtained without any additives or post-treatments. Better miscibility was observed in **PQTE/PC₇₁BM** blend film compared with that of **PQ2T/PC₇₁BM** blend film although strong interchain interaction existed in polymer **PQTE**. We suppose that good intercalation of **PC₇₁BM** into the lamellar structure of **PQTE** responsible for this high PCE. Our findings indicate that rational molecular modification makes quinacridone to be a promising building block applied in high-performance optoelectronic devices.

Experimental section

Materials and synthesis

5,5'-Bis(trimethylstannyl)-2,2'-bithiophene and (*E*)-1,2-bis(5-(trimethylstannyl)thiophene-2-yl)ethene were purchased from Suna Tech Inc. and without further purification. All other chemicals were purchased from Aldich and used as received. Number-average and weight-average were determined by gel permeation chromatography (GPC) on a Waters 515 chromatograph connected to a Waters 2410 refractive index detector, using THF as eluent and polystyrene standards as calibrants. Thermogravimetric analysis (TGA) measurements were recorded by Shimadzu thermogravimetric analyzer (model DTG-60) under a nitrogen flow, heating from room temperature to 800 °C, with a heating rate of 10 °C min⁻¹. Differential scanning calorimetry (DSC) analyses were performed on a METTLER TOLEDO Instrument with DSC822 calorimeter. UV-vis absorption spectra were measured on a Shimadzu UV-3600 UV-VIS-NIR spectrophotometer. Cyclic voltammetric experiments were carried out in a conventional three-electrode cell consisting of a platinum working electrode coated with a thin film layer of polymer, a platinum wire auxiliary electrode, and an Ag/AgCl reference electrode with ferrocenium-ferrocene (Fc⁺-Fc) as the internal standard. Tetrabutylammoniumhexafluorophosphate (TBAPF₆) (0.1 M) was used as the supporting electrolyte. Atom force microscopy (AFM) was investigated by Bruker Multimode 8 using tapping mode with a scan speed of 1 Hz. Transmission electron microscopy (TEM) was performed on a JEM-2011 operated at 100 kV. Grazing incidence X-ray diffraction (GIXRD) data were obtained at 1W1A, Beijing Synchrotron Radiation Facility. The films were illuminated at a constant incidence angle of 0.2° ($\lambda = 2d\sin\theta = 1.5464 \text{ Å}$).

Synthesis of PQTE. Monomer QA2Br (150 mg, 0.131 mmol) and (*E*)-1,2-bis(5-(trimethylstannyl)thiophene-2-yl)ethene (68

mg, 0.131 mmol) were added into a Schlenk tube and subsequently dissolved in 6 mL degassed chlorobenzene. The solution degassed before Pd₂(dba)₃ (2.4 mg, 0.003 mmol) and P(*o*-tol)₃ (6.4 mg, 0.021 mmol) were added. The reaction mixture was further degassed and subsequently sealed. The solution was heated and stirred at 130 °C for 48 h. After cooling to room temperature, the mixture was added to vigorously stirred methanol and filtered. The resulting precipitate was purified by Soxhlet extraction successively with methanol, acetone, hexane, and finally with chloroform, and then precipitated in methanol again. The polymer PQTE was obtained as purple solids (167 mg, 78%).

Synthesis of PQ2T. The similar procedure as described above was used to synthesize PQ2T (171 mg, 80%).

General procedure for devices fabrication

OFET devices fabrication and characterization. Bottom-gate/top-contact FET devices were fabricated on SiO₂/Si substrates. First, the substrates were cleaned and treated with octadecyltrichlorosilane (OTS). Polymer solution in chlorobenzene (6 mg mL⁻¹) was spin coated at a speed of 2000 rpm for 50 s to obtain film with thickness of ~ 35 nm. The samples were further placed on a hot plate at 150 °C in N₂ for 30 min. Gold source and drain electrodes (60 nm) were deposited by vacuum evaporation on the organic layer through a shadow mask. The channel length (*L*) and width (*W*) were 30 μm and 500 μm, respectively. OFETs were determined at room temperature in air by using a Keithley 4200 SCS (semiconductor characterization system). The mobility of the OTFTs in the saturation region was extracted from the following equation: $I_{DS} = C_i \mu (W/2L)(V_G - V_T)^2$, where I_{DS} is the drain current, C_i is the capacitance of the SiO₂ dielectric layer ($C_i = 10$ nF cm⁻²), μ is field-effect hole mobility, V_G and V_T are the gate voltage and threshold voltage, respectively.

OPV devices fabrication and characterization. For conventional devices of ITO/PEDOT:PSS/polymer/PC₇₁BM/Ca/Al, the ITO substrates were cleaned and exposed to a 30 min UV/O₃ treatment, and then PEDOT:PSS (2000 rpm for 30 min) was spin-coated and followed by a thermal annealing treatment at 150 °C for 15 min. After cooling to room temperature, the chlorobenzene solution of polymer/PC₇₁BM mixture was spin-coated at a speed of 1000 rpm for 30 s. Then Ca/Al cathode was successively deposited on photoactive layer by vacuum evaporation (20 nm/80 nm). The current-voltage (*J-V*) characteristics of the devices were measured by using a Keithley 2400 Source Measure Unit. The measurements were conducted under the irradiation of AM 1.5 G, 100 mW cm⁻². EQE measurements were carried out on an oriel IQE 200 (Newport).

Acknowledgements

This work was supported by the National Natural Science Foundation of China (Nos. 21073200, 91222203, 21273251, 21373239, 91333111, 21190034, 21221002), project of Construction of Innovative Teams and Teacher Career

Development for Universities and Colleges Under Beijing Municipality (IDHT20140512), the National Basic Research Program of China (973) 2011CB808402, 2013CB933500, and the Chinese Academy of Sciences. We thank the Beijing Synchrotron Radiation Facility (beamline 1W1A) for providing the beam time.

Notes and references

^a Beijing National Laboratory for Molecular Science (BNLMS), Institute of Chemistry, Chinese Academy of Science, Beijing 100190, P. R. China. Fax: +86-10-62526801; Tel: +86-10-62526801; E-mail: hongbing.fu@iccas.ac.cn.

^b University of Chinese Academy of Sciences, Beijing 100049, P. R. China.

^c Beijing Key Laboratory for Optical Materials and Photonic Devices, Department of Chemistry, Capital Normal University, Beijing 100048, P. R. China.

† Electronic Supplementary Information (ESI) available: GPC analysis, TGA, DSC results, DFT calculation, AFM images, 2D-GIXRD profiles. See DOI: 10.1039/b000000x/

- 1 Y. J. Cheng, S. H. Yang and C. S. Hsu, *Chem. Rev.*, 2009, **109**, 5868-5923.
- 2 P. M. Beaujuge and J. M. Frechet, *J. Am. Chem. Soc.*, 2011, **133**, 20009-20029.
- 3 T. Lei, Y. Cao, X. Zhou, Y. Peng, J. Bian and J. Pei, *Chem. Mater.*, 2012, **24**, 1762-1770.
- 4 I. Meager, R. S. Ashraf, S. Rossbauer, H. Bronstein, J. E. Donaghey, J. Marshall, B. C. Schroeder, M. Heeney, T. D. Anthopoulos and I. McCulloch, *Macromolecules*, 2013, **46**, 5961-5967.
- 5 L. Pandey, C. Risko, J. E. Norton and J.-L. Brédas, *Macromolecules*, 2012, **45**, 6405-6414.
- 6 J. D. Yuen and F. Wudl, *Energy & Environ. Sci.*, 2013, **6**, 392-406.
- 7 K. H. Hendriks, G. H. L. Heintges, V. S. Gevaerts, M. M. Wienk and R. A. J. Janssen, *Angew. Chem. Int. Ed.*, 2013, **52**, 8341-8344.
- 8 S. Zhang, L. Ye, W. Zhao, D. Liu, H. Yao and J. Hou, *Macromolecules*, 2014, **47**, 4653-4659.
- 9 P. Liu, K. Zhang, F. Liu, Y. Jin, S. Liu, T. P. Russell, H.-L. Yip, F. Huang and Y. Cao, *Chem. Mater.*, 2014, **26**, 3009-3017.
- 10 J. Li, Y. Zhao, H. S. Tan, Y. Guo, C.-A. Di, G. Yu, Y. Liu, M. Lin, S. H. Lim, Y. Zhou, H. Su and B. S. Ong, *Sci. Rep.*, 2012, **2**, 754-756.
- 11 I. Kang, H.-J. Yun, D. S. Chung, S.-K. Kwon and Y.-H. Kim, *J. Am. Chem. Soc.*, 2013, **135**, 14896-14899.
- 12 G. Kim, S.-J. Kang, G. K. Dutta, Y.-K. Han, T. J. Shin, Y.-Y. Noh and C. Yang, *J. Am. Chem. Soc.*, 2014, **136**, 9477-9483.
- 13 I. Osaka, M. Shimawaki, H. Mori, I. Doi, E. Miyazaki, T. Koganezawa and K. Takimiya, *J. Am. Chem. Soc.*, 2012, **134**, 3498-3507.
- 14 H.-Z. Gao, *Int. J. Quantum Chem.*, 2012, **112**, 740-746.
- 15 T. L. Chen, J. J.-A. Chen, L. Catane and B. Ma, *Org. Electron.*, 2011, **12**, 1126-1131.
- 16 I. Javed, T. Zhou, F. Muhammad, J. Guo, H. Zhang and Y. Wang, *Langmuir*, 2012, **28**, 1439-1446.
- 17 M. Sytnyk, E. D. Glowacki, S. Yakunin, G. Voss, W. Schöfberger, D. Krieger, J. Stangl, R. Trotta, C. Gollner, S. Tollabimazraehno, G. Romanazzi, Z. Bozkurt, M. Havlicek, N. S. Sariciftci and W. Heiss, *J. Am. Chem. Soc.*, 2014, **136**, 16522-16532.

- 18 E. D. Głowacki, M. Irimia-Vladu, M. Kaltenbrunner, J. Gąsiorowski, M. S. White, U. Monkowius, G. Romanazzi, G. P. Suranna, P. Mastrorilli, T. Sekitani, S. Bauer, T. Someya, L. Torsi and N. S. Sariciftci, *Adva. Mater.*, 2013, **25**, 1563-1569.
- 19 I. Osaka, M. Akita, T. Koganezawa and K. Takimiya, *Chem. Mater.*, 2012, **24**, 1235-1243.
- 20 I. Javed, Z. Zhang, T. Peng, T. Zhou, H. Zhang, M. Issa Khan, Y. Liu and Y. Wang, *Solar Energy Mater. Solar Cells*, 2011, **95**, 2670-2676.
- 21 T. V. Pho, H. Kim, J. H. Seo, A. J. Heeger and F. Wudl, *Adv. Funct. Mater.*, 2011, **21**, 4338-4341.
- 22 T. Zhou, T. Jia, B. Kang, F. Li, M. Fahlman and Y. Wang, *Adv. Energy Mater.*, 2011, **1**, 431-439.
- 23 H.-J. Song, D.-H. Kim, E.-J. Lee, S.-W. Heo, J.-Y. Lee and D.-K. Moon, *Macromolecules*, 2012, **45**, 7815-7822.
- 24 H.-J. Song, D.-H. Kim, E.-J. Lee and D.-K. Moon, *J. Mater. Chem. A*, 2013, **1**, 6010-6020.
- 25 H. Li, C. Gu, L. Jiang, L. Wei, W. Hu and H. Fu, *J. Mater. Chem. C*, 2013, **1**, 2021-2027.
- 26 H. Li, Y. Wu, X. Wang, Q. Kong and H. Fu, *Chem. Commun.*, 2014, **50**, 11000-11003.
- 27 H. J. Song, D. H. Kim, E. J. Lee, J. R. Haw and D. K. Moon, *Solar Energy Mater. Solar Cells*, 2014, **123**, 112-121.
- 28 H.-J. Yun, H. H. Choi, S.-K. Kwon, Y.-H. Kim and K. Cho, *Chem. Mater.*, 2014, **26**, 3928-3937.
- 29 E. H. Jung and W. H. Jo, *Energy Environ Sci*, 2014, **7**, 650-654.
- 30 J. Shin, H. A. Um, D. H. Lee, T. W. Lee, M. J. Cho and D. H. Choi, *Polym. Chem.*, 2013, **4**, 5688-5695.
- 31 D. Qian, L. Ye, M. Zhang, Y. Liang, L. Li, Y. Huang, X. Guo, S. Zhang, Z. a. Tan and J. Hou, *Macromolecules*, 2012, **45**, 9611-9617.
- 32 J. Mei, D. H. Kim, A. L. Ayzner, M. F. Toney and Z. Bao, *J. Am. Chem. Soc.*, 2011, **133**, 20130-20133.
- 33 L. Dou, J. You, J. Yang, C.-C. Chen, Y. He, S. Murase, T. Moriarty, K. Emery, G. Li and Y. Yang, *Nat. Photon.*, 2012, **6**, 180-185.
- 34 I. Osaka, R. Zhang, G. Sauvé, D.-M. Smilgies, T. Kowalewski and R. D. McCullough, *J. Am. Chem. Soc.*, 2009, **131**, 2521-2529.
- 35 W. Li, A. Furlan, W. S. C. Roelofs, K. H. Hendriks, G. W. P. van Pruissen, M. M. Wienk and R. A. J. Janssen, *Chem. Commun.*, 2014, **50**, 679-681.
- 36 S. J. Woo, E. Kim and Y. H. Lee, *Phys. Rev. B*, 1993, **47**, 6721-6727.
- 37 A. C. Mayer, M. F. Toney, S. R. Scully, J. Rivnay, C. J. Brabec, M. Scharber, M. Koppe, M. Heeney, I. McCulloch and M. D. McGehee, *Adv. Funct. Mater.*, 2009, **19**, 1173-1179.
- 38 N. C. Cates, R. Gysel, Z. Beiley, C. E. Miller, M. F. Toney, M. Heeney, I. McCulloch and M. D. McGehee, *Nano Lett.*, 2009, **9**, 4153-4157.